Geophysical Journal International

Geophys. J. Int. (2020) **220,** 393–403 doi: 10.1093/gji/ggz453
Advance Access publication 2019 October 07
Rock and Mineral Physics, Rheology

On the Green function of the Lord–Shulman thermoelasticity equations

Zhi-Wei Wang,[1,2,3] Li-Yun Fu,[4] Jia Wei,[1,2,3] Wanting Hou,[4] Jing Ba[5] and José M. Carcione[6]

[1]*Key Laboratory of Petroleum Resource Research, Institute of Geology and Geophysics, Chinese Academy of Sciences, Beijing* 100029*, P. R. China. E-mail:* wzw@mail.iggcas.ac.cn
[2]*Innovation Academy for Earth Science, CAS, Beijing* 100029*, P. R. China*
[3]*University of Chinese Academy of Sciences, Beijing* 100049*, P. R. China*
[4]*Key Laboratory of Deep Oil and Gas, China University of Petroleum (East China), Qingdao* 266580*, P. R. China.*
[5]*School of Earth Sciences and Engineering, Hohai University, Nanjing* 211100*, P. R. China*
[6]*Istituto Nazionale di Oceanografia e di Geofisica Sperimentale (OGS), Borgo Grotta Gigante* 42c*, Sgonico, Trieste* 34010*, Italy*

Accepted 2019 October 5. Received 2019 September 22; in original form 2019 June 3

SUMMARY

Thermoelasticity extends the classical elastic theory by coupling the fields of particle displacement and temperature. The classical theory of thermoelasticity, based on a parabolic-type heat-conduction equation, is characteristic of an unphysical behaviour of thermoelastic waves with discontinuities and infinite velocities as a function of frequency. A better physical system of equations incorporates a relaxation term into the heat equation; the equations predict three propagation modes, namely, a fast *P* wave (*E* wave), a slow thermal *P* wave (*T* wave), and a shear wave (*S* wave). We formulate a second-order tensor Green's function based on the Fourier transform of the thermodynamic equations. It is the displacement–temperature solution to a point (elastic or heat) source. The snapshots, obtained with the derived second-order tensor Green's function, show that the elastic and thermal *P* modes are dispersive and lossy, which is confirmed by a plane-wave analysis. These modes have similar characteristics of the fast and slow *P* waves of poroelasticity. Particularly, the thermal mode is diffusive at low thermal conductivities and becomes wave-like for high thermal conductivities.

Key words: Fourier analysis; Numerical solutions; Seismic attenuation; Wave propagation.

1 INTRODUCTION

Thermoelasticity is an extension of classical elasticity, which deals with the interaction between the displacement and temperature fields (Lord & Shulman 1967; Green & Lindsay 1972; Green & Naghdi 1993; Tzou 1995; Hetnarski & Ignaczak 1997; Chandrasekharaiah 1998). The study of wave propagation in a thermoelastic solid is of fundamental importance in several disciplines such as seismic exploration (Zener 1938; Treitel 1959; Savage 1966; Armstrong 1984), geothermal studies (Jacquey *et al*. 2015), earthquake seismology (Boschi 1973) and others (Tsai 2011; Auriault 2014). Hetnarski & Ignaczak (1999) explain the difference theories in terms of the input properties and predicted waves.

The theory of thermoelasticity has been established by Biot (1956) on the basis of the thermodynamics of irreversible process. Deresiewicz (1957) applies a plane-wave analysis to investigate propagation of waves in an isotropic thermoelastic solid. Three kinds of waves propagate, namely, *E* wave, *T* wave and *S* wave. The *T* wave has been observed in experimental measurements for some specific materials. Ackerman *et al*. (1966) observed it in solid helium, while McNelly *et al*. (1970) and Jackson *et al*. (1970) detected the *T* wave in NaF crystals. However, the longitudinal *E* and *T* waves predicted by Biot and Deresiewicz have infinite velocities at infinite frequencies, since the classical thermoelastic equations are based on a parabolic-type heat transfer equation. This anomalous behaviour can be avoided by introducing a relaxation term into the heat equation (e.g. Vernotte 1948; Lord & Shulman 1967; Green & Lindsay 1972; Turchetti & Mainardi 1976; Ignaczak & Ostoja-Starzewski 2010). Banerjee & Pao (1974) investigate the propagation of plane harmonic waves in anisotropic media. Nowacki (1975) constructs the thermodynamic foundation of thermoelasticity systematically and develops the Green function for anisotropic media, based on the classical thermoelasticity equation with the unrealistic infinite velocity. Similarly, Tosaka (1985) derives Green's function for boundary-element analyses based on the same thermoelasticity equation. Rudgers (1990) studies the characteristic of thermoelastic waves as a function of frequency. Norris (1994) describes a procedure to generate fundamental solutions or the Green functions for time harmonic point forces and sources for the theories of piezoelectricity, thermoelasticity and poroelasticity. Bear *et al.* (1992) and Sharma (2008) investigate the theory of thermo-poroelasticity. To our knowledge, Carcione *et al.* (2018, 2019) are the first to simulate thermoelastic and thermo-poroelastic wave propagation with realistic propagation velocities, including a relaxation term in the heat equation, that is, the Lord–Shulman theory and its generalization to the poroelastic case. The algorithm is based on the Fourier pseudospectral method, with the simulations showing the thermal wave and the Biot slow wave.

Many researchers have used Green's function to study wave propagation in elastic or viscoelastic media, but with few studies on the Green function in thermoelastic media. The fundamental solutions for the case of isotropic thermoelasticity arekg $\mathrm{s}^{-3}\,\mathrm{K}^{-1}$ known (Kupradze *et al.* 1976). Tosaka & Suh (1991) formulate the Green function based on the classical thermoelastic theory (a parabolic-type heat equation). Here, we obtain the Green function of the thermoelasticity equations with one relaxation time, based on the theory of Lord & Shulman (1967) (a hyperbolic-type heat equation). Fundamental solutions (or Green's functions) play an important role in the numerical solution of partial differential equations by integral equation methods, and as a test of numerical solutions. First, we analyse the characteristic of the wave propagation in thermoelastic media by a plane-wave method, the theory predicts two distinct lossy longitudinal waves, that is, *E* wave and *T* wave, whereas the predicted S wave is unaffected by the thermal effects. Then, we formulate the integral equation of the modified thermoelasticity equations (Hörmander 2013) in the frequency domain and obtain the second-order tensor Green's function corresponding to point loadings (force or heat sources) in a homogeneous isotropic material. Finally, we calculate wavefield snapshots to analyse displacements and temperatures, corresponding to vertical and horizontal loadings (heat sources).

2 EQUATIONS OF THERMOELASTICITY

Biot (1956) and Deresiewicz (1957) establish the relations between stress, strain and temperature in linear isotropic media. However, their equations lack the relaxation term in the heat equation, leading to physically unacceptable solutions for the *T* wave (i.e. infinite phase velocity). The modified thermoelasticity equations with a relaxation term are (e.g. Carcione *et al*. 2018) written by using the Einstein implicit summation as follows:

Strain–displacement relations:

$$\epsilon_{ij} = \frac{1}{2}\left(u_{i,j} + u_{j,i}\right), \tag{1}$$

where u_i and ϵ_{ij} are the components of displacement and strain, respectively.

Stress–strain relations for isotropic media

$$\sigma_{ij} = 2\mu\epsilon_{ij} + \lambda\delta_{ij}u_{k,k} - \beta\delta_{ij}T + f_{ij}, \tag{2}$$

where σ_{ij} are the stress components, λ and μ are the Lamé constants, δ_{ij} are the Kronecker-delta components, f_{ij} are external stress forces, T is the increment of temperature above a reference absolute temperature T_0, and $\beta = (3\lambda + 2\mu)\alpha$ with α being the coefficient of thermal expansion. Eq. (2) indicates that the temperature-induced elastic variations in stress strongly depend on the coefficient of thermal expansion.

Equations of momentum conservation:

$$\sigma_{ji,j} = \rho\ddot{u}_i + f_i, \tag{3}$$

where f_i are the components of external body forces, ρ is the mass density and a dot above a variable denotes time differentiation.

Law of hear conduction:

$$\gamma\Delta T = c\left(\dot{T} + \tau\ddot{T}\right) + T_0\beta\left(\dot{u}_{k,k} + \tau\ddot{u}_{k,k}\right) + q, \tag{4}$$

where γ is the coefficient of thermal conductivity, c is the specific heat of the unit volume in the absence of deformation, τ is a relaxation time, q is a heat source and Δ is the Laplacian operator. The resultant temperature gradient that leads to heat transfer depends not only on the heat source but also on the strain rate at each point of the elastic body. A relaxation time τ is introduced to make the heat equation hyperbolic, leading to wave-like behaviour for the *T* wave.

By combining eqs (1)–(4), we obtain

$$\begin{cases} \mu u_{i,jj} + (\lambda + \mu)u_{j,ji} - \beta\, T_{,i} = \rho\ddot{u}_i, \\ \gamma\, T_{,jj} = c\left(\dot{T} + \tau\ddot{T}\right) + T_0\beta\left(\dot{u}_{j,j} + \tau\ddot{u}_{j,j}\right) + q \end{cases}. \tag{5}$$

Eq. (5) couples the mechanical and thermal motions. The strain and temperature fields are coupled as a result of the action of elastic and heat sources. *S* waves are not affected by the temperature, since the shear strain is not coupled with the heat equation. On the other hand, the *P* wave generates temperature gradients leading to mechanical energy dissipation and heat-conduction absorption, while the heat equation predicts a *T* wave analogous to the slow *P* wave of Biot theory of poroelasticity. In fact, the static constitutive equations of poroelasticity and thermoelasticity are formally the same if we identify the pore-fluid pressure with the temperature and the fluid compression with entropy (Norris 1991).

3 DISPERSION ANALYSES WITH PLANE WAVES

A plane-wave analysis of the thermoelasticity equations provides a simple way to understand the physics of wave propagation in thermoelastic media. Let us consider the following plane-wave expression of the displacement components and temperature fluctuations,

$$\begin{cases} u_i = Ad_i \exp\left[\mathrm{i}\omega\left(t - sl_ix_i\right)\right], \\ T = B \exp\left[\mathrm{i}\omega\left(\left(t - sl_ix_i\right)\right)\right], \end{cases} \tag{6}$$

where ω is the angular frequency, t is the time, $s = 1/V_\mathrm{c}$ is the slowness with V_c being the complex velocity, d_i is a unit vector denoting the direction of displacement, x_i is the position components, l_i is the directions defining the propagation direction, A and B are amplitude constants, and $\mathrm{i} = \sqrt{(-1)}$.

3.1 Dispersion relations

For the S wave, $d_i\, l_i = 0$ (Deresiewicz 1957), that is, the direction of displacement is perpendicular to the propagation direction. As formulated in Appendix B, we obtain the following dispersion relation for this wave:

$$\begin{cases} \left[\mu\left(\frac{\omega}{V_\mathrm{c}}\right)^2 - \rho\omega^2\right] A - \mathrm{i}\frac{\omega}{V_\mathrm{c}}\beta B = 0, \\ \left[\mathrm{i}\omega c - \omega^2\tau + \gamma\left(\frac{\omega}{V_\mathrm{c}}\right)^2\right] B = 0. \end{cases} \tag{7}$$

The solution to this equation results in the S-wave velocity,

$$B = 0, \; V_\mathrm{c} = \sqrt{\mu/\rho}. \tag{8}$$

We see that the S-wave propagation is lossless because of the isotropic assumption in the current thermoelasticity theory, where the shear stresses are independent of temperature, and therefore they are not coupled with the heat-conduction equation. Likewise, for P waves, $d_i\, l_i = 1$ (Deresiewicz 1957), that is, the direction of displacement is parallel to the propagation direction. As described in Appendix B, we obtain the following dispersion relation:

$$\left[-\rho\omega^2 + (\lambda + 2\mu)\left(\frac{\omega}{V_\mathrm{c}}\right)^2\right]\left[\mathrm{i}c\omega + \gamma\left(\frac{\omega}{V_\mathrm{c}}\right)^2 - c\tau\omega^2\right] = -\beta^2\gamma\, T_0\frac{\omega}{V_\mathrm{c}}\left(\mathrm{i}\omega - \tau\omega^2\right). \tag{9}$$

The solution to this equation results in complex velocities for the P waves,

$$2V_\mathrm{c}^2 = V_\mathrm{A}^2 + M \pm \sqrt{\left(V_\mathrm{A}^2 + M\right)^2 - 4V_\mathrm{I}^2 M}. \tag{10}$$

where $M = \mathrm{i}\omega a^2/(1 + \mathrm{i}\omega\tau)$, with $a = \sqrt{(\gamma/c)}$, is a complex kernel arising from a Maxwell mechanical model of viscoelasticity (Carcione 2014), $V_\mathrm{I} = \sqrt{((\lambda+2\mu)/\rho)}$ and $V_\mathrm{A} = \sqrt{(V_\mathrm{I}{}^2 + b^2)}$, with $b = \beta\sqrt{(T_0/(\rho c)}$, are the isothermal and adiabatic phase velocities (Rudgers 1990; Carcione *et al.* 2018). We see that the P-wave propagation is dissipative because of the coupling of the bulk stresses with the heat-conduction equation. There are two longitudinal waves, an elastic E wave (a fast P wave) and a T wave (a slow thermal P wave). We have two real solutions for $\omega = 0$,

$$V_\mathrm{c} = 0 \;(\mathrm{T\ wave}), \quad V_\mathrm{c} = V_\mathrm{A} \;(\mathrm{E\ wave}). \tag{11}$$

For $c \rightarrow \infty$, we have $V_\mathrm{c} = V_\mathrm{I}$, whereas for $\gamma \rightarrow 0$, we obtain $V_\mathrm{c} = V_\mathrm{A}$. For $\gamma \rightarrow \infty$ or $\omega \rightarrow \infty$, V_c becomes the high-frequency limit E-wave velocity $V_{\mathrm{E}\infty}$ and limit T-wave velocity $V_{\mathrm{T}\infty}$, respectively. A detailed discussion on the values of τ associated with relaxation peaks and peak frequencies are given in Carcione *et al.* (2018).

3.2 Dispersion and attenuation behaviour

The model with the thermoelastic properties, $\rho = 2600$ kg m^{-3}, $\lambda = 4$ GPa, $\mu = 6$ GPa, $T_0 = 318$ K, $\alpha = 4.09 \times 10^{-6}$ K^{-1} and $c = 104$ m s^2 K^{-1}. We consider two cases for the thermal conductivity, one with $\gamma = 2.61$ m kg s^{-3} K^{-1} typical of rocks and the other with a higher value of $\gamma = 4.5 \times 10^4$ m kg s^{-3} K^{-1} to illustrate the physics. The phase velocity $V_\mathrm{p} = [\mathrm{Re}(1/V_\mathrm{c})]^{-1}$, and the attenuation coefficient $A_\mathrm{c} = -4\pi\,\mathrm{Im}(1/V_\mathrm{c})V_\mathrm{p}$ can be calculated from the complex velocity V_c, as a function of frequency (see Carcione 2014).

Figs 1 and 2 show the phase velocities and attenuation coefficients of the elastic and thermal waves as a function of frequency for the two values of the thermal conductivity, respectively. The inflexion point of the velocity occurs at a frequency $f_\mathrm{p} = V_\mathrm{I}{}^2/(2\pi a^2)$, nearly at 39 MHz in the first case and 2.26 KHz in the second case. As can be seen, the E wave low-frequency velocity is the adiabatic one, that is, $V_\mathrm{A} = 3553$ m s^{-1}, whereas $V_\mathrm{I} = 2481$ m s^{-1}, the isothermal velocity, is not involved in the coupled case. The high-frequency E wave limit velocity is $V_{\mathrm{E}\infty} = 4059$ m s^{-1}, the high-frequency T wave limit velocity is $V_{\mathrm{T}\infty} = 1516$ m s^{-1}, close to the S-wave velocity.

Because of the thermoelastic due to heat diffusion, the E and T waves are attenuated and undergo dispersion. Note that the attenuation coefficients of the two waves have a peak ($A_\mathrm{c} \approx 1$), in both cases at the angular frequency $\omega \approx 1/\tau$, depending on the values of γ (Rudgers

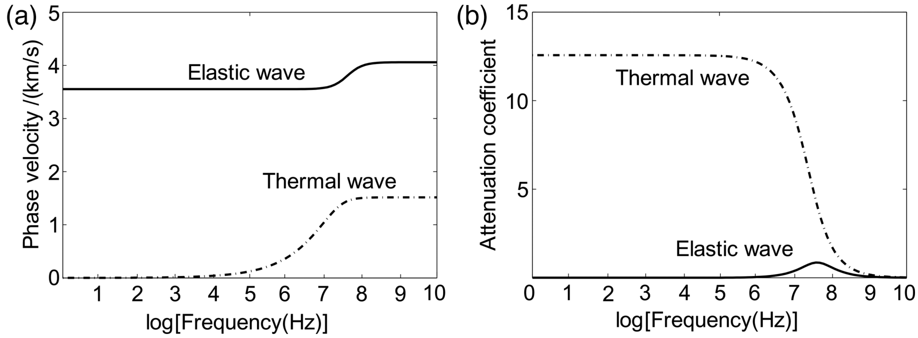

Figure 1. Phase velocities (a) and attenuation coefficients (b) of the *E* and *T* waves as a function of frequency for the thermal conductivity $\gamma = 2.61$ m kg s^{-3} K^{-1}.

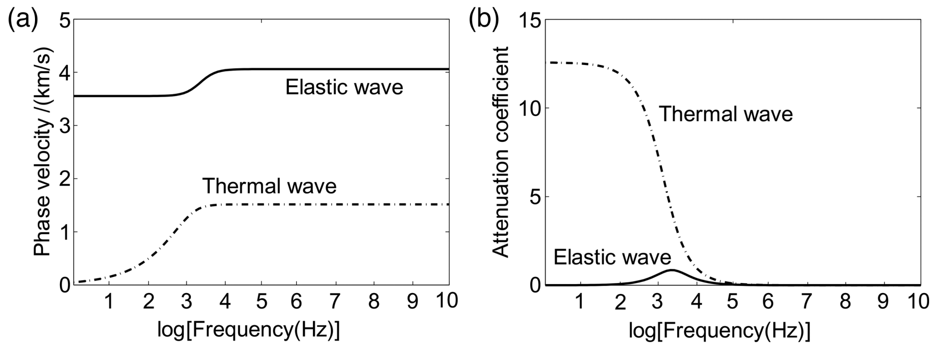

Figure 2. Phase velocities (a) and attenuation coefficients (b) of *E* and *T* waves as a function of frequency for the thermal conductivity $\gamma = 4.5 \times 10^4$ m kg s^{-3} K^{-1}.

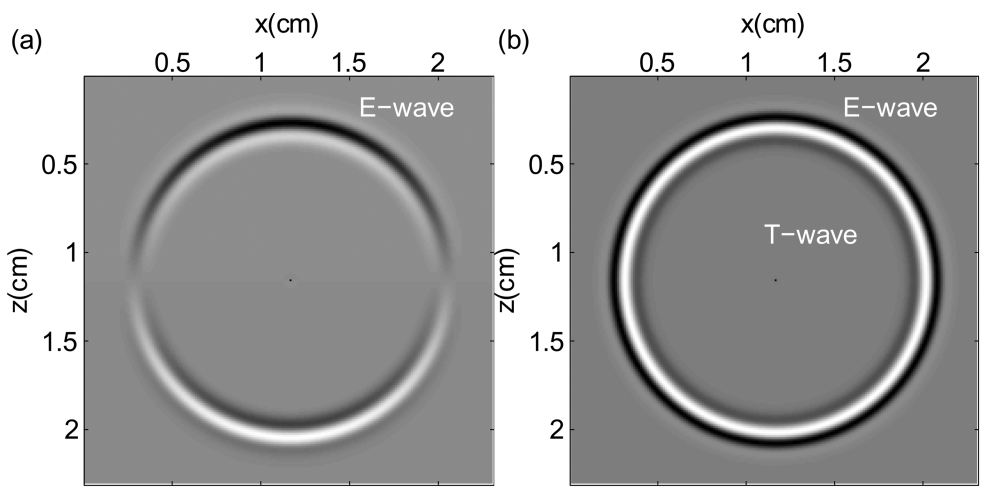

Figure 3. Snapshots of the vertical component of the particle velocity (a) and temperature (b) at 3 μs, corresponding to the coupled case with $\gamma = 10.5$ m kg s^{-3} K^{-1}. The perturbation is a heat source with a central frequency of 3.5 MHz.

1990). We obtain a peak at the ultrasonic band for values of γ typical of rocks. Increasing τ, the peak moves to low frequencies. The timescale for heat diffusion is a function of the length scale involved in the process of heat flow. The behaviour of the *T* wave has similar characteristics to that of the Biot slow diffusive wave. The mathematical analogy identifies temperature field in thermoelasticity with fluid pressure in poroelasticity (Bonnet 1987; Manolis & Beskos 1989; Norris 1991).

The thermal conductivity γ ranges from 24 000 m kg s^{-3} K^{-1} for CRC aluminium to 0.023 m kg s^{-3} K^{-1} for air, whereas rocks filled with fluids have a range between 1 and 12 m kg s^{-3} K^{-1}. We select two very dissimilar values, namely, $\gamma = 2.6$ m kg s^{-3} K^{-1} and $\gamma = 4.5 \times 10^4$ m kg s^{-3} K^{-1}, to show how the physics behaves.

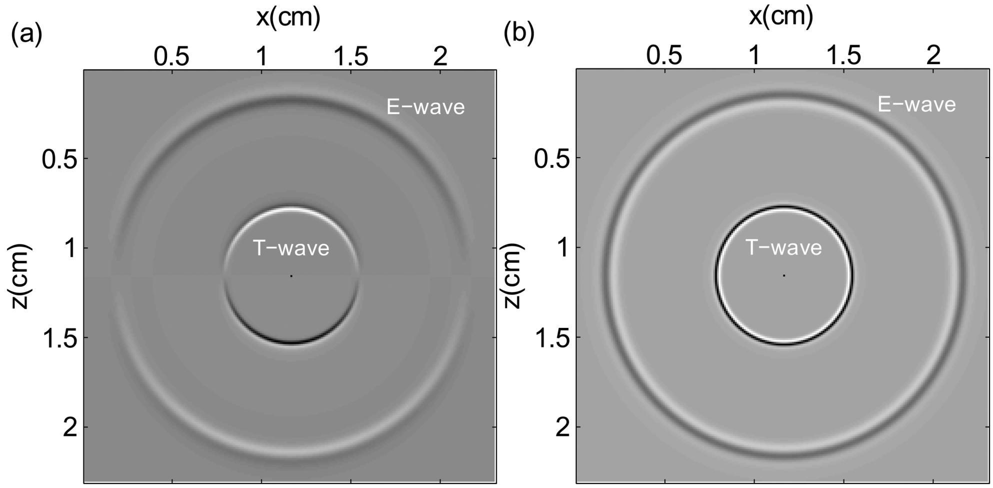

Figure 4. Snapshots of the vertical component of the particle velocity (a) and temperature (b) at 3 μs, corresponding to the coupled case with a high thermal conductivity of $\gamma = 4.5 \times 10^6$ m kg s^{-3} K^{-1}. The perturbation is a heat source with a central frequency of 3.5 MHz.

4 GREEN'S FUNCTIONS

Green's functions represent the fundamental solution to partial differential equations with a point source (the force or heat source). The Green function of the classical thermoelasticity theory (a parabolic-type equation) has been derived for a homogeneous isotropic medium (Tosaka & Suh 1991). In this section, we formulate the Green function of the modified thermoelasticity equations with a relaxation term (Lord & Shulman 1967). The derived process generally consists of three steps (e.g. Pao & Varatharajulu 1976): structuring the fundamental equation for the solution of partial differential equations to a point source, solving the fundamental equation by variables separation method and reconstructing the fundamental solution tensor

4.1 Fundamental equation

Applying the Fourier transform defined by

$$\tilde{u}\ (\mathbf{x}, \omega) = \int_0^\infty u\,(\mathbf{x}, t)\ \mathrm{e}^{-\mathrm{i}\omega t}\mathrm{d}t, \tag{12}$$

to eq. (5), we obtain the following differential equations in the frequency domain (omitting the hat for convenience):

$$\begin{cases} \mu u_{i,jj} + (\lambda + \mu)\, u_{j,ji} + \rho\omega^2 u_i - \beta\ T_{,i} = 0, \\ \gamma T_{,jj} - c\left(i\omega - \tau\omega^2\right) T - T_0\beta\left(\mathrm{i}\omega - \tau\omega^2\right)\ u_{j,j} = 0. \end{cases} \tag{13}$$

It is convenient to rewrite the above system in the following matrix form:

$$L_{ij}\ U_j = 0, \tag{14}$$

where

$$L_{ij} = \begin{vmatrix} \mu\Delta + (\lambda+\mu)\, D_1^2 + \rho\omega^2 & (\lambda+\mu)\, D_1 D_2 & -\beta D_1 \\ (\lambda+\mu)\, D_1 D_2 & \mu\Delta + (\lambda+\mu)\, D_1^2 + \rho\omega^2 & -\beta D_2 \\ -T_0\beta\left(\mathrm{i}\omega - \tau\omega^2\right) D_1 & -T_0\beta\left(\mathrm{i}\omega - \tau\omega^2\right) D_2 & \gamma\Delta - \mathrm{c}\left(\mathrm{i}\omega - \tau\omega^2\right) \end{vmatrix},$$

and

$$U_j = \left\langle \tilde{u}_1\ \ \tilde{u}_2\ \ \tilde{T} \right\rangle,$$

with the notation $D_i = \partial/\partial x_i$ (i = 1,2).

The fundamental solution tensor (a weighting tensor as the basic components of Green's function) $V_{ij}{}^*$ satisfies the differential equation to a point source,

$$L^*_{ij} V^*_{jk} = -\delta^*_{ik}\delta\,(x - y)\,, \tag{15}$$

where $L_{ij}{}^*$ is the adjoint cofactor operator of L_{ij}.

$$L^*_{ij} = \begin{vmatrix} \mu\Delta + (\lambda+\mu)\, D_1^2 + \rho\omega^2 & (\lambda+\mu)\, D_1 D_2 & -T_0\beta\left(\mathrm{i}\omega - \tau\omega^2\right) D_1 \\ (\lambda+\mu)\, D_1 D_2 & \mu\Delta + (\lambda+\mu)\, D_1^2 + \rho\omega^2 & -T_0\beta\left(\mathrm{i}\omega - \tau\omega^2\right) D_2 \\ -\beta D_1 & -\beta D_2 & \gamma\Delta - \mathrm{c}\left(\mathrm{i}\omega - \tau\omega^2\right) \end{vmatrix}$$

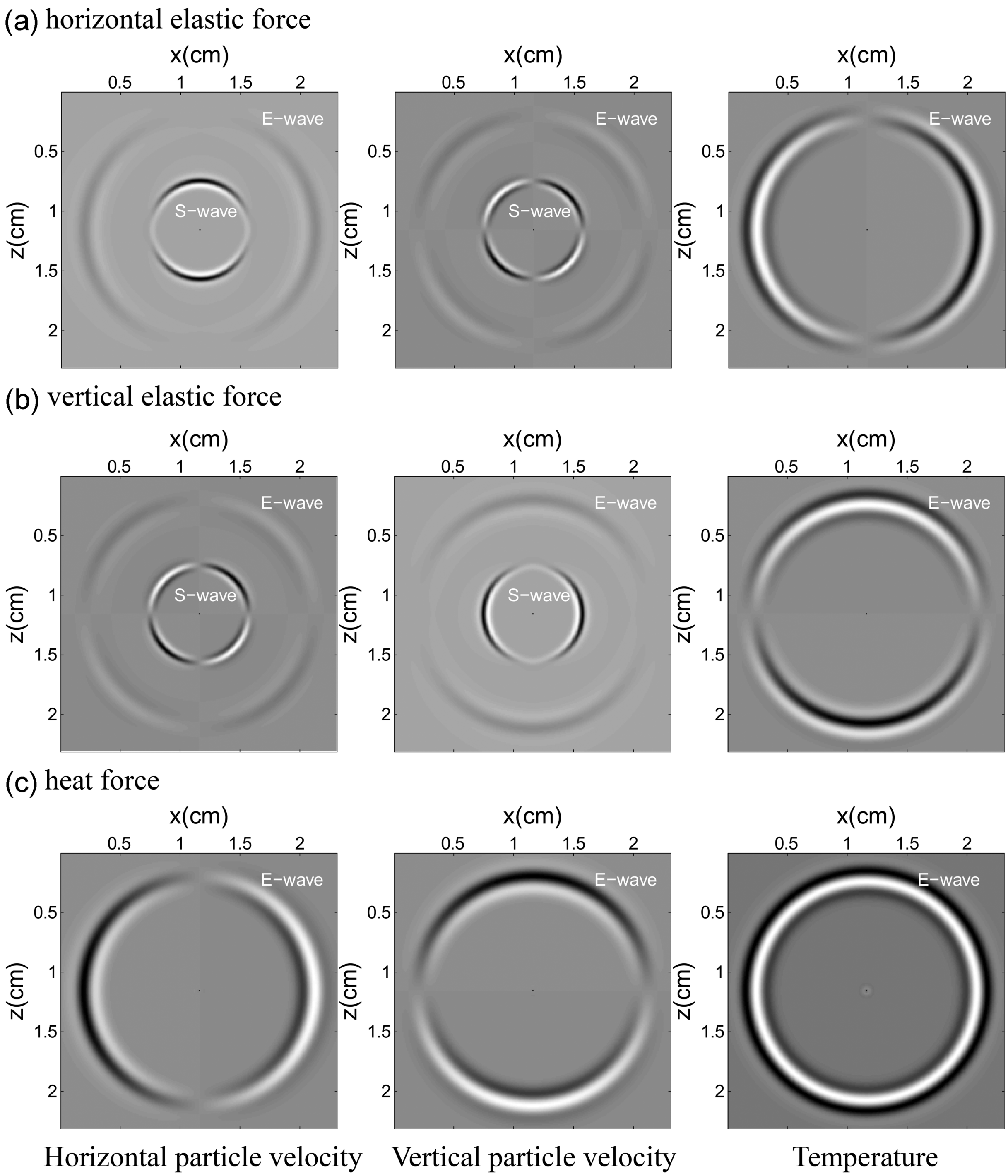

Figure 5. Snapshots of the horizontal particle velocity (left panel), vertical particle velocity (middle panel) and temperature (right panel) at 2.6 μs, calculated for a thermal conductivity of $\gamma = 2.61$ m kg s^{-3} K^{-1}, with a horizontal elastic force (a), a vertical elastic force (b) and a heat source (c), corresponding to a Ricker-wavelet frequency of $f_0 = 1.5$ MHz.

4.2 Fundamental solutions

In order to derive the solution to eq. (15), we follow Kupradze *et al.* (1976) and Tosaka & Suh (1991) and make use of the fundamental solution tensor V_{ij}^* in terms of the scalar potential function Φ^* and the transposed co-factor operator $L_{ij}{}^{\mathrm{T}}$ of $L_{ij}{}^*$.

$$V_{ij}^* \,(x, y, s) = L_{ij}^T \, \Phi^* \,(x, y, s) \,. \tag{16}$$

Substitution of eq. (16) into eq. (15) yields

$$\Lambda \, \Phi^* = \; - \, \delta \,(x - y) \,, \tag{17}$$

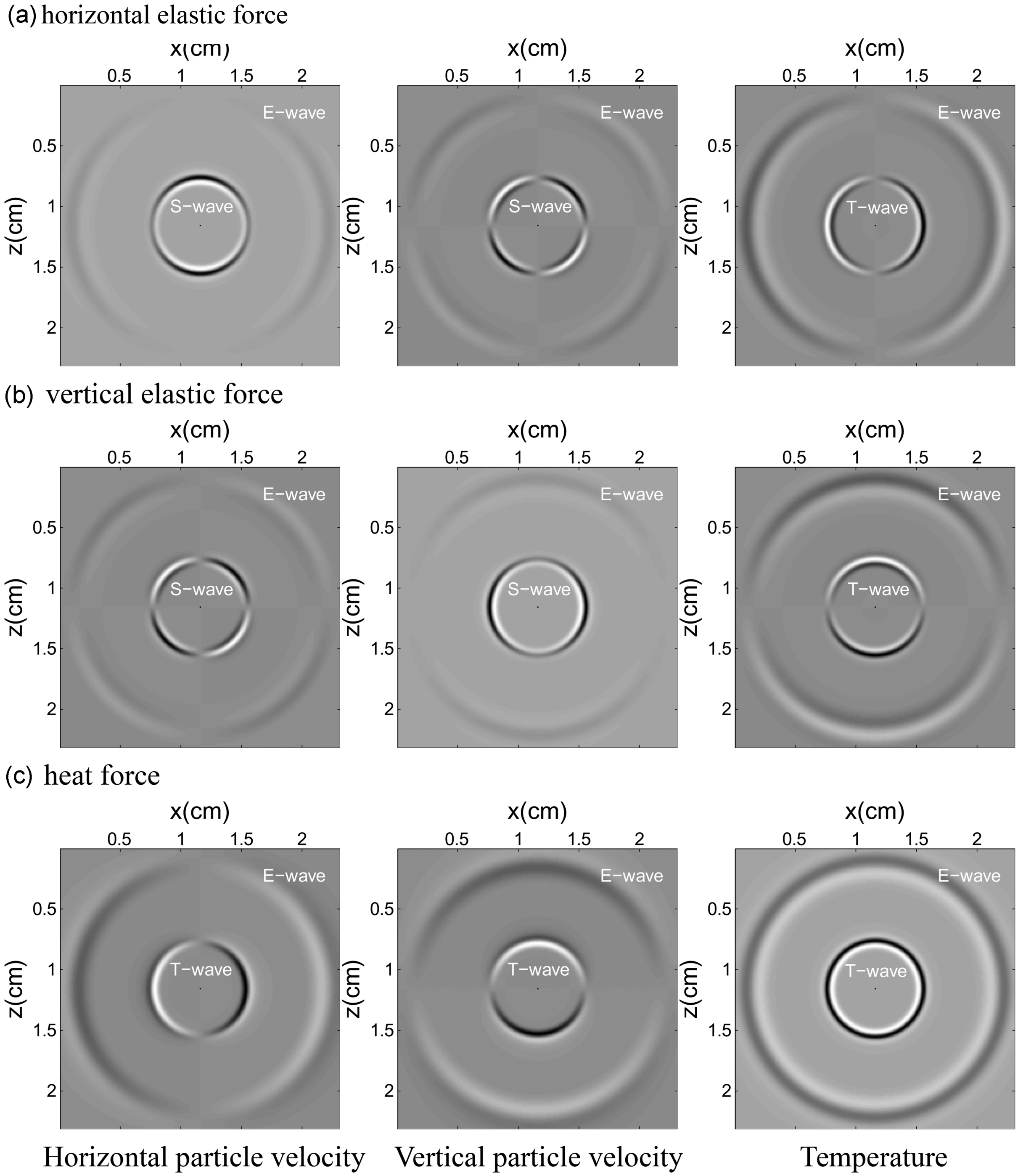

Figure 6. Snapshots of the horizontal particle velocity (left panel), vertical particle velocity (middle panel) and temperature (right panel) at 2.6 μs, calculated with the thermal conductivity $\gamma = 4.5 \times 10^4$ m kg s^{-3} K^{-1}, for a horizontal elastic force (a), a vertical elastic force (b) and a heat source (c) corresponding to a Ricker-wavelet frequency of $f_0 = 1.5$ MHz.

where

$$\Lambda \ = \ \det \left(L^*_{ij}\right) = \frac{\mu}{\lambda + 2\mu} \ \left(\Delta - h_1^2\right)\left(\Delta - h_2^2\right)\left(\Delta - h_3^2\right), \tag{18}$$

and the coefficient of $h_i{}^2$ can be determined as these which satisfy

$$\begin{cases} h_1^2 + h_2^2 = \frac{\rho\omega^2}{\lambda+2\mu} - \frac{\mathrm{i}\omega(1+\mathrm{i}\omega\tau)}{\kappa}\left(1 + \frac{\beta^2 T_0}{c(\lambda+2\mu)}\right), \\ h_1^2 h_2^2 = -\frac{\rho\omega^2}{\lambda+2\mu} \cdot \frac{\mathrm{i}\omega(1+\mathrm{i}\omega\tau)}{\kappa}, \\ h_3^2 = \frac{\rho\omega^2}{\mu}. \end{cases} \tag{19}$$

Note that h_1 and h_2 are functions of the relaxation time τ, while, h_3 and τ are not related.

Using eq. (18), the fundamental solution for Φ^* from eq. (17) can be formulated as

$$\Phi^* = \frac{\lambda + 2\mu}{2\pi\mu} \sum_{i=1}^{3} W_i K_0 (\mathrm{i} h_i r), \tag{20}$$

where

$$W_i = \frac{-1}{\left(h_i^2 - h_j^2\right)\left(h_k^2 - h_i^2\right)} \quad (i = 1, 2, 3\ j = 2, 3, 1\ k = 3, 1, 2). \tag{21}$$

Each component of the fundamental solution tensor $V_{ij}{}^*$ can be obtained by employing the derived fundamental solution as follows:

$$\begin{cases} V_{ij}^* = \frac{1}{2\pi\mu} W_k \sum_{k=1}^{3} \left(\psi_k(r)\delta_{ij} - \chi_k(r) r_{,i} r_{,j}\right), & (i, j = 1, 2), \\ V_{3i}^* = \frac{\beta}{2\pi(\lambda+2\mu)} \sum_{k=1}^{3} W_k \xi_k(r) r_{,i}, & (i = 1, 2), \\ V_{i3}^* = \frac{\mathrm{i}\omega\eta}{2\pi(\lambda+2\mu)} \sum_{k=1}^{3} W_k \xi_k(r) r_{,i}, & (i = 1, 2), \\ V_{33}^* = \frac{1}{2\pi} \sum_{k=1}^{3} W_k \zeta_k(r), \end{cases} \tag{22}$$

where

$$\begin{cases} \psi_k(r) = \left[\left(h_k^2 + m\right)\left(h_k^2 - m_1\right) + \frac{\eta\beta\kappa m h_k^2}{\lambda+2\mu}\right] K_0(\mathrm{i}h_k r) - P_k \frac{h_k}{r} K_1(\mathrm{i}h_k r), \\ \chi_k(r) = P_k h_k^2 K_2(\mathrm{i}h_k r), \\ \xi_k(r) = -\left(h_k^2 - m_2\right) \mathrm{i}h_k K_1(\mathrm{i}h_k r), \\ \zeta_k(r) = \left(h_k^2 - m_1\right)\left(h_k^2 - m_2\right) K_0(\mathrm{i}h_k r), \end{cases} \tag{23}$$

with

$$P_k = \frac{\lambda + \mu}{\lambda + 2\mu}\left(h_k^2 + m\right), \tag{24}$$

and

$$m = \frac{\mathrm{i}\omega(1 + \mathrm{i}\omega\tau)}{\kappa}, \quad m_1 = \frac{\rho\omega^2}{\lambda + 2\mu}, \quad m_2 = \frac{\rho\omega^2}{\mu}, \quad \kappa = \frac{\gamma}{c}, \quad \eta = \frac{\beta T_0}{\gamma}. \tag{25}$$

Here, K_0, K_1 and K_2 are the modified Bessel function of the second kind of order zero, first and second, respectively, with the argument $r = \| x - y \|$.

To understand the physical meaning of the basic components of the Green function (i.e. fundamental solution tensor), it is convenient to write the fundamental solution in matrix form as

$$V_{ij}^* = \begin{vmatrix} V_{11}^* & V_{12}^* & V_{13}^* \\ V_{21}^* & V_{22}^* & V_{23}^* \\ V_{31}^* & V_{32}^* & V_{33}^* \end{vmatrix}. \tag{26}$$

This Green function is a second-order tensor with nine components, where ($V_{11}{}^*$, $V_{21}{}^*$, $V_{31}{}^*$), ($V_{12}{}^*$, $V_{22}{}^*$, $V_{32}{}^*$) and ($V_{13}{}^*$, $V_{23}{}^*$, $V_{33}{}^*$) correspond to the horizontal particle velocity, vertical particle velocity and temperature, respectively, of a horizontal elastic force, a vertical elastic force, and a heat source, respectively.

4.3 Numerical experiments

We use the analytical method, based on the proposed second-order tensor Green's function (eq. 22), to calculate wavefield snapshots, where the model parameters are consistent with those used in Carcione *et al.* (2018). The source is a vertical force and has the time function $h(t) = \cos[(t - t_0) f_0]\ \exp[-2(t - t_0)^2 f_0{}^2]$, where the central frequency is $f_0 = 3.5$ MHz and $t_0 = 3/(2f_0)$ is a delay time.

Fig. 3 shows the vertical particle velocity (a) and temperature field (b) for a heat source, with $\gamma = 10.5$ m kg s^{-3} K^{-1}. As expected, there is no *S* wave. The velocity of the *E* wave is slightly less than $V_{\mathrm{E}\infty}$, whereas the *T* wave is diffusive. As predicted by Fig. 1(b), the *T* wave is highly attenuated and can hardly be seen.

Fig. 4 shows the vertical particle velocity (a) and temperature field (b) for a heat source, corresponding to $\gamma = 4.5 \times 10^6$ m kg s^{-3} K^{-1}. The *E* and *T* wave fronts travel with the velocities $V_{\mathrm{E}\infty}$ and $V_{\mathrm{T}\infty}$, respectively. The difference with Fig. 3 is the weak attenuation of the *T* wave, in agreement with Fig. 2(b).

To compare snapshots generated by the elastic and heat sources, we consider a 231 × 231 mesh with square cells and a grid spacing of $dx = dz = 100$ μm. The source is a Ricker wavelet located at the centre of the mesh with $f_0 = 1.5$ MHz. The model thermoelastic properties are same as those in Section 3.2. Fig. 5 shows snapshots of the horizontal particle velocity (left panel), vertical particle velocity (middle panel) and temperature (right panel) are calculated at 2.6 μs according to eq. (26), with $\gamma = 2.61$ m kg s^{-3} K^{-1}, for a horizontal elastic force (a), a vertical elastic force (b) and a heat source (c). The *E* (i.e. fast *P* wave) and *S* waves have their motions consistent with the radiation pattern for point forces (Aki & Richards 2002). The velocity of the *E* wave is slightly less than $V_{E\infty}$. The *T* wave is highly attenuated according to Fig. 1(b).

Fig. 6 shows snapshots of the particle velocity and temperature tensor for $\gamma = 4.5 \times 10^4$ m kg s^{-3} K^{-1} along the *x*- and *z*-directions for a Ricker-wavelet frequency of $f_0 = 1.5$ MHz. The snapshots of the horizontal particle velocity (left panel), vertical particle velocity (middle panel) and temperature (right panel) are calculated at 2.6 μs, according to eq. (26), for a horizontal elastic force (a), a vertical elastic force (b) and a heat source (c). The *E* and *S* waves have their motions consistent with the radiation pattern for point forces (Aki & Richards 2002). The *E* and *T* wave fronts travel with the velocities $V_{E\infty}$ and $V_{T\infty}$. We can see the *T* wave, since the attenuation is negligible, in agreement with Fig. 2(b).

5 CONCLUSIONS

We have considered the modified thermoelasticity equations that incorporate a relaxation term to overcome the unphysical behaviour described by the classical theory. We formulate a second-order tensor Green's function for wave propagation in a homogeneous isotropic medium. It is the displacement–temperature solution to a point (elastic or heat) source. The Green function is generally used as the fundamental solution for the integral equation representation of thermoelasticity problems and a test of numerical algorithms. The theory predicts three distinct waves: an *E* wave (a fast *P* wave), a *T* wave (a thermal *P* wave) and an *S* wave (a shear wave). The *P* waves suffer attenuation and velocity dispersion because of the compression/expansion-induced temperature gradients leading to mechanical energy dissipation and heat conduction, whereas the *S* wave is unaffected by the thermal effects.

We compare the heat-source-induced wavefield snapshots of the vertical particle velocity and temperature by assuming a very high thermal conductivity with a smaller one typical of rocks. In the latter case, the *T* wave has a diffusive character, whereas it is wave-like for a much higher conductivity. For a heat source, there are no *S* waves. We also compare snapshots of the horizontal/vertical particle velocities and temperature generated by horizontal/vertical elastic forces and heat source. These numerical experiments show that the elastic and thermal *P* modes are dispersive and lossy, as predicted by the plane-wave analyses. These modes have similar characteristics of the fast and slow *P* waves of the poroelasticity theory. In particular, the thermal mode is diffusive at low thermal conductivities and becomes wave-like for high thermal conductivities. In poroelasticity, this corresponds to high and low fluid viscosities.

A detailed account of the boundary integral equation formulation and implementation by boundary-element numerical methods using the Green function presented here will be the subject of a future paper.

ACKNOWLEDGEMENTS

Valuable comments by Rene-Edouard Plessix, Sven Treitel and anonymous reviewer significantly improved the paper. The work presented here was supported by the Major State Research Development Program of China (Grant No. 2016YFC0601101) and the Strategic Priority Research Program of the Chinese Academy of Science projects (Grant No. XDA10010403) and PetroluemChina Project (Grant No. 2016A-4801).

REFERENCES

Ackerman, C.C., Bertman, B., Fairbank, H.A. & Guyer, R.A., 1966. Second sound in solid helium, *Phys. Rev. Lett.,* **16,** 789–791.

Aki, K. & Richards, P.G. 2002. *Quantitative Seismology,* 2nd edn, University Science Books.

Armstrong, B.H., 1984. Models for thermoelastic attenuation of waves in heterogeneous solids, *Geophysics,* **49,** 1032–1040.

Auriault, J.L., 2014. Inner thermal resonance in thermoelastic geological structures, *Acta Geophys.,* **62,** 993–1004.

Banerjee, D.K. & Pao, Y.H., 1974. Thermoelastic waves in anisotropic solids, *J. acoust. Soc. Am.,* **56,** 1444–1454.

Bear, J., Sorek, S., Ben-Dor, G. & Mazor, G., 1992. Displacement waves in saturated thermoelastic porous media. I. Basic equations, *Fluid. Dyn. Res.,* **9,** 155–164.

Biot, M.A., 1956. Thermoelasticity and irreversible thermodynamics, *J. Appl. Phys.,* **27,** 240–253.

Bonnet, G., 1987. Basic singular solutions for a poroelastic medium in the dynamic range, *J. acoust. Soc. Am.,* **82,** 1758–1762.

Boschi, E., 1973. A thermoviscoelastic model of the earthquake source mechanism, *J. geophys. Res.,* **78,** 7733–7737.

Carcione, J.M., 2014. *Wave FIelds in Real Media: Wave Propagation in Anisotropic, Anelastic, Porous and Electromagnetic Media,* Elsevier.

Carcione, J.M., Wang, Z.W., Ling, W., Salusti, E., Ba, J. & Fu, L.Y., 2018. Simulation of wave propagation in linear thermoelastic media, *Geophysics,* **84,** T1–T11.

Carcione, J.M., Cavallini, F., Wang, E., Ba, J. & Fu, L.Y., 2019. Simulation of wave propagation in linear thermo-poroelastic media, *J. geophys. Res.,* in press.

Chandrasekharaiah, D.S., 1998. Hyperbolic thermoelasticity: a review of recent literature, *Appl. Mech. Rev.,* **51,** 705–729.

Deresiewicz, H., 1957. Plane waves in a thermoelastic solid, *J. acoust. Soc. Am.,* **29,** 204–209.

Hetnarski, R.B. & Ignaczak, J., 1997. On solition-like thermoelastic waves, *Appl. Anal.,* **65,** 183–204.

Hetnarski, R.B. & Ignaczak, J., 1999. Generalized thermoelasticity, *J. Therm. Stresses,* **22,** 451–476.

Hörmander, L., 2013. *Linear Partial Differential Operators,* Springer.

Jackson, H.E., Walker, C.T. & McNelly, T.F., 1970. Second sound in NaF, *Phys. Rev. Lett.,* **25,** 26–28.

Jacquey, A.B., Cacace, M., Blöcher, G. & Scheck-Wenderoth, M., 2015. Numerical investigation of thermoelastic effects on fault slip tendency during injection and production of geothermal fluids, *Energy Procedia,* **76,** 311–320.

Ignaczak, J. & Ostoja-Starzewski, M., 2010. *Thermoelasticity with Finite Wave Speeds,* Oxford University Press.

Green, A.E. & Lindsay, K.A., 1972. Thermoelasticity, *J. Elast.,* **2,** 1–7.

Green, A.E. & Naghdi, P.M., 1993. Thermoelasticity without energy dissipation, *J. Elast.,* **31,** 189–208.

Kupradze, V.D., Gegelia, T.G., Basheleishvili, M.O. & Burchuladze, T.V., 1976. *Three-Dimensional Problems of the Mathematical Theory of Elasticity and Thermoelasticity,* North-Holland.

Lord, H.W. & Shulman, Y., 1967. A generalized dynamical theory of thermoelasticity, *J. Mech. Phys. Solids,* **15,** 299–309.

Manolis, G.D. & Beskos, D.E., 1989. Integral formulation and fundamental solutions of dynamic poroelasticity and thermoelasticity, *Acta Mech.,* **76,** 89–104.

McNelly, T.F., Rogers, S.J., Channin, D.J., Rollefson, R.J., Goubau, W.M., Schmidt, G.E. & Pohl, R.O., 1970. Heat pulses in NaF: onset of second sound, *Phys. Rev. Lett.,* **24,** 100–102.

Norris, A.N., 1991. On the correspondence between poroelasticity and thermoelasticity, *J. Appl. Phys.,* **71,** 1138–1141.

Norris, A.N., 1994. Dynamic Green's functions in anisotropic piezoelectric, thermoelastic and poroelastic solids, *Proc. R. Soc. A,* **447,** 175–188.

Nowacki, W., 1975. *Dynamic problems of Thermoelasticity,* Springer Science & Business Media.

Pao, Y.H. & Varatharajulu, V., 1976. Huygens' principle, radiation conditions, and integral formulas for the scattering of elastic waves, *J. acoust. Soc. Am.,* **59,** 1361–1370.

Rudgers, A.J., 1990. Analysis of thermoacoustic wave propagation in elastic media, *J. acoust. Soc. Am.,* **88,** 1078–1094.

Savage, J.C., 1966. Thermoelastic attenuation of elastic waves by cracks, *J. geophys. Res.,* **71,** 3929–3938.

Sharma, M.D., 2008. Wave propagation in thermoelastic saturated porous medium, *J. Earth Syst. Sci.,* **117,** 951–958.

Tosaka, N., 1985. The integral equation formulation for boundary-value problems by the coupled system of differential equations (in Japanese), *Japan NCTAM,* 323–324.

Tosaka, N. & Suh, I.G., 1991. Boundary element analysis of dynamic coupled thermoelasticity problems, *Comput. Mech.,* **8,** 331–342.

Treitel, S., 1959. On the attenuation of small-amplitude plane stress waves in a thermoelastic solid, *J. geophys. Res.,* **64,** 661–665.

Tsai, V.C., 2011. A model for seasonal changes in GPS positions and seismic wave speeds due to thermoelastic and hydrologic variations, *J. geophys. Res.,* **116**.

Turchetti, G. & Mainardi, F., 1976. Wave front expansions and Padé approximants for transient waves in linear dispersive media,H.Cabannes, in *Padé Approximants Method and Its Applications to Mechanics,* Springer, pp. 189–207.

Tzou, D.Y., 1995. A unified field approach for heat conduction from macro-to micro-scales, *J. Heat Transfer,* **117,** 8–16.

Vernotte, P., 1948. Théorie continue et théorie moléculaire des phénomènes thermocinétiques, *C. R. Acad. Sci.,* **227,** 43–44.

Zener, C., 1938. Internal friction in solids II. General theory of thermoelastic internal friction, *Phys. Rev.,* **53,** 90–99.

APPENDIX A: LIST OF SYMBOLS

u_i	Components of the displacement ($i = 1, 2, 3$)
ϵ_{ij}	Strain components ($i, j = 1, 2, 3$)
σ_{ij}	Stress components ($i, j = 1, 2, 3$)
λ, μ	Lamé constants
δ_{ij}	Kronecker-delta component
f_{ij}	External stress forces ($i, j = 1, 2, 3$)
T_0	Absolute temperature for the state of zero stress and strain
T	Increment of temperature above a reference absolute temperature T_0
α	Coefficient of thermal expansion
β	Stress–temperature modulus
f_i	Components of the external body forces ($i = 1, 2, 3$)
ρ	Mass density
γ	Coefficient of heat conduction (or thermal conductivity)
c	Specific heat of the unit volume in the absence of deformation
τ	Relaxation time
q	Heat source
Δ	Laplacian operator
ω	Angular frequency
V_c	Complex velocity
s	Slowness
d_i	Directions of the displacement vector ($i = 1, 2, 3$)
x_i	Position components ($i = 1, 2, 3$)
l_i	The propagation direction ($i = 1, 2, 3$)
A, B	Amplitude constants
a	Thermal diffusivity
V_I	Isothermal phase velocities
V_A	Adiabatic phase velocities

Note: Subscript 'i' denotes a spatial derivative.

APPENDIX B: VELOCITY OF THE *S* AND *P* WAVES IN A HOMOGENEOUS THERMOELASTIC MEDIUM

To derive the *P* and *S* wave velocities, we use eq. (6) to obtain the following functions related to displacement and temperature,

$$\begin{cases} u_{i,jj} = -\left(\frac{\omega}{V_c}\right)^2 Ad_i, \; u_{j,ji} = -\left(\frac{\omega}{V_c}\right)^2 Ad_j l_j l_i, \; \ddot{u}_i = -\omega^2 Ad_i, \\ T_{,jj} = -\left(\frac{\omega}{V_c}\right)^2 B, \; \ddot{u}_{j,j} = \mathrm{i}\frac{\omega}{V_c}\omega^2 Ad_j l_j, \; \dot{u}_{j,j} = \frac{\omega}{V_c}\omega Ad_j l_j, \\ T_{,i} = -\mathrm{i}\frac{\omega}{V_c} Bl_i, \; \dot{T} = \mathrm{i}\omega B, \; \ddot{T} = -\omega^2 B, \end{cases} \tag{B1}$$

where the exponential term is omitted for the sake of brevity. Substituting eq. (B1) into eq. (5), we obtain a system of algebraic equations

$$\begin{cases} \mu\left(\frac{\omega}{V_c}\right)^2 Ad_i - \rho\omega^2 Ad_i + (\lambda+\mu)\left(\frac{\omega}{V_c}\right)^2 Ad_j l_j l_i - i\gamma B\beta\, l_i = 0, \\ c\left(\mathrm{i}\omega B - \tau\omega^2 B\right) + T_0\beta\left(\frac{\omega}{V_c}\omega Ad_j l_j + \mathrm{i}\tau\frac{\omega}{V_c}\omega^2 Ad_j l_j\right) + \gamma\left(\frac{\omega}{V_c}\right)^2 B = 0. \end{cases} \tag{B2}$$

For the *S* wave, $d_i\, l_i = 0$ and eq. (B2) reduces to

$$\begin{cases} \left[\mu\left(\frac{\omega}{V_c}\right)^2 - \rho\omega^2\right] A - i\frac{\omega}{V_c}\beta B = 0, \\ \left[\mathrm{i}\omega c - \omega^2\tau + \gamma\left(\frac{\omega}{V_c}\right)^2\right] B = 0. \end{cases} \tag{B3}$$

The solution to this equation for the *S*-wave velocity is

$$B = 0, \; V_c = \sqrt{\mu/\rho}\,. \tag{B4}$$

For the *P* wave, $d_i\, l_i = 1$ and eq. (B2) reduces to

$$\begin{cases} \left[-\rho\omega^2 + (\lambda+2\mu)\left(\frac{\omega}{V_c}\right)^2\right] A = i\beta\frac{\omega}{V_c} B, \\ i\beta T_0\frac{\omega}{V_c}\left(\mathrm{i}\omega - \tau\omega^2\right) A = \left(\mathrm{i}c\omega + \gamma\left(\frac{\omega}{V_c}\right)^2 - c\tau\omega^2\right) B. \end{cases} \tag{B5}$$

Eliminating the constants A and B leads to the secular equation

$$\left[-\rho\omega^2 + (\lambda+2\mu)\left(\frac{\omega}{V_c}\right)^2\right]\left[\mathrm{i}c\omega + \gamma\left(\frac{\omega}{V_c}\right)^2 - c\tau\omega^2\right] = -\beta^2\gamma\, T_0\frac{\omega}{V_c}\left(\mathrm{i}\omega - \tau\omega^2\right). \tag{B6}$$

By introducing the variables $a = \surd(\gamma/c)$, $b = \beta\,\surd(T_0/(\rho c)$ and $V_I = \surd((\lambda+2\mu)/\rho)$, $V_A = \surd(V_I{}^2 + b^2)$, we have

$$\left(-V_c^2 + V_A^2\right)\mathrm{i}\omega\left(1 + \mathrm{i}\tau\omega\right) + \left[-V_c^2 + V_I^2\right] a^2 \left(\frac{\omega}{V_c}\right)^2 = 0. \tag{B7}$$

Defining $M = (\mathrm{i}\omega a^2)/(1 + \mathrm{i}\tau\omega)$, eq. (B7) can be further written as

$$V_c^4 - \left(V_A^2 + M\right) V_c^2 + V_I^2 M = 0. \tag{B8}$$

The solution to this equation for the *P*-wave velocity is

$$2V_c^2 = V_A^2 + M \pm \sqrt{\left(V_A^2 + M\right)^2 - 4V_I^2 M}. \tag{B9}$$